Contents lists available at ScienceDirect

Displays

journal homepage: www.elsevier.com/locate/displa

CDMS: A Real-Time System for EEG-Guided Cybersickness Mitigation Through Adaptive Adjustment of VR Content Factors

Ufuk Uyan, Ufuk Celikcan*

Hacettepe University, Department of Computer Engineering, Ankara, Turkey

ARTICLE INFO

Communicated by

Keywords:
Virtual Reality
Cybersickness Mitigation
EEG
Head Mounted Displays
Content Factors
Stereoscopy
Convolutional Neural Networks

ABSTRACT

Cybersickness remains a major issue that can severely impact the user's comfort, performance, and enjoyment of VR. While there are various approaches to combat cybersickness, only a few have been developed for real-time mitigation based on user biofeedback, and these do not aim to distinguish causal factors and apply mitigation accordingly. In this paper, we propose a novel real-time cybersickness detection and mitigation system (CDMS) that leverages a two-stage shallow convolutional network to detect cybersickness and identify the contributing factors from the user's electroencephalogram (EEG) activity. Based on the output of the convolutional network, CDMS adaptively modifies the parameters of the identified factor in the generated virtual environment to mitigate the onset cybersickness. For this, we conjointly consider three major content factors of cybersickness: navigation speed, scene complexity, and stereoscopic rendering. To train the network, we collected EEG data and self-reports of cybersickness from the subjects by simulating these factors in varying degrees of severity. For the performance evaluation of CDMS, we conducted a user study comprising one CDMS session and two different control sessions. The results show that the users experienced significantly less cybersickness after the CDMS session. Also, CDMS effectively avoided false positives that could otherwise degrade the VR experience.

1. Introduction

Despite the significant breakthroughs in virtual reality (VR) technologies, viewers immersed in virtual environments (VEs) with state-of-the-art setups are still susceptible to experiencing cybersickness. Previous studies have shown that 30% [1] to 80% [2] of viewers are prone to the ailment. Identifying cybersickness can be challenging due to its various symptoms, including nausea, cold sweats, dizziness, headache, increased salivation, and fatigue, which can vary from person to person. Even though the hardware-related limitations, such as lag, tracking accuracy, and flicker, which were once regarded as the primary sources of discomfort felt in VEs [3], have been considerably alleviated with the latest head mounted displays (HMDs), the sickness experienced remains the most notorious aspect associated with VR [4, 5]. In this work, we propose a novel system to mitigate the cybersickness experienced with VR-HMDs in real-time via the adjustment of VR content factors based on the user's brain activity.

Among the myriad of reasons ranging from physical conditions to individual differences [6], the sensory conflict is widely seen as the leading cause of cybersickness [7]. The sensory conflict theory, as outlined by Reason and Brand [8], suggests that cybersickness results from conflicts between sensory informa-

*Corresponding author: E-mail:celikcan@cs.hacettepe.edu.tr; Tel.: +90-312-297-7500;

http://dx.doi.org/10.1016/j.displa.xxxx.xx.xxx
Received ; Received in final form ; Accepted ; Available online
0141-9382/

tion from different receptors, as well as conflicts between current sensory perception and expected sensory patterns, whereby conflicts between sensory information modulate the perception-expectation conflict [7, 9]. In VR-HMDs, visual causes dominate cybersickness symptoms due to visual-vestibular conflicts or conflicts between visual cues [10]. Visual-vestibular conflicts occur when there is mismatch between the visually perceived motion and the sense of bodily motion. Further, the visually perceived motion in a VE can also be discomforting in relation to scene complexity [11]. Another prevailing cause is the vergence-accommodation conflict (VAC), which arises due to the discrepancy between the perceived depth and the focus depth of the eyes [12]. In stereoscopic VR headsets, a focused object is displayed on the HMD in very close proximity to the eyes, but the perceived depth of the object varies with the stereoscopic rendering parameters [13]. Although most people are able to tolerate VAC to some degree [14], excessive mismatch can contribute to focusing problems, visual fatigue, and eyestrain, especially with prolonged use. In addition, VAC can contribute to the visual-vestibular conflict through the confusion of depth perception [10]. Our work focuses on three VR content factors, namely navigation speed, level of scene complexity, and stereoscopic rendering parameters, which are among the major content factors of cybersickness in relation to the aforementioned conflicts [10, 15, 16]. We propose a framework to mitigate cybersickness through automated manipulation of these factors as needed.

Three methods are frequently used to grade cybersickness. The most common one is the use of questionnaires. The Simulator Sickness Questionnaire (SSQ) proposed by Kennedy et al. [17] is widely utilized in cybersickness studies due to the similarity of symptoms to simulator sickness [15]. Another method is the measurement of postural sway, based on the theory that postural imbalance predicts cybersickness [18]. However, recent findings have contradicted this theory [19, 20] and some studies have reported results in favor of the sensory conflict theory rather than postural instability [21]. Therefore, the most recent guidelines do not recommend using postural instability as a criterion or predictor of cybersickness [10]. Lastly, biofeedback can be used to detect the onset of cybersickness and grade its severity. Brain activity has been recognized as a comprehensive biofeedback to detect cybersickness and associated cognitive load [22–24]. Kim et al. [25] showed that the indices of autonomic nervous system activity offer reliable measures of cybersickness. In this study, we measured brain activity using EEG signals via a wireless mobile headset (Emotiv Epoc+), which grants ease of application in addition to timely biofeedback and multiple spatial components from different electrodes. EEG data has been shown to be useful in identifying and mitigating cybersickness [26], as it can be measured without interrupting immersion [27] and provides ample feedback directly from brain regions linked to cybersickness.

Most studies on cybersickness have focused solely on assessment, with limited research on mitigation. Only a few studies have explored real-time mitigation based on user biofeedback [28, 29], and the approaches used have aimed at detecting cybersickness without distinguishing between causal factors. Our proposed framework comprises a two-stage neural network classifier to detect the onset of cybersickness and identify the dominant content trigger by analyzing the user's brain activity during VR immersion. This allows for adaptive adjustment of only the relevant content factor parameters in the presented VE. So that, as the factor is classified using the EEG signal with a high sampling rate, the VE is modified with low latency through continuous and smooth tuning of the factoring parameters to maintain immersion and presence.

The main contributions of this work are as follows:

- We propose the Cybersickness Detection and Mitigation System (CDMS), which operates during a VR experience in real-time based on the user's brain activity in the form of EEG signals.
- To our knowledge, the proposed approach is the first to consider three major VR content factors of cybersickness (navigation speed, scene complexity, and stereoscopic rendering parameters) together for a real-time cybersickness mitigation system. To this end, CDMS incorporates a novel VE that simulates these cybersickness factors and adaptively tunes them based on EEG feedback.
- Two separate neural network models, based on the Shallow ConvNet architecture [30], are trained for CDMS. The first model detects the onset of cybersickness with an overall accuracy of 76.26%. The second model classifies the dominant content factor causing the onset with an overall accuracy of 81.01%.
- We evaluate the performance of CDMS against two different control schemes. The results show that CDMS achieves satisfactory performance in mitigating cybersickness without the need for individual calibration.

In the following, we first give an overview of the previous work in Section 2. Then, Section 3 presents our methodology for real-time cybersickness mitigation using brain activity response, detailing the components of CDMS and data collection. Section 4 describes our CDMS evaluation experiment along with the report of the results and their discussion. Finally, the limitations of our work are outlined in Section 5 and Section 6 concludes the paper.

2. Previous Work

Cybersickness research has garnered particular attention in recent years as the use of virtual and augmented reality systems has shifted from a niche market of experienced users to general consumers. In Rebenitsch et al.'s review of cybersickness [15], possible factors considered to cause cybersickness were compared and measurement methods that are used to determine the severity of symptoms were investigated. Kolasinski et al. [31] proposed over 40 possible cybersickness factors, which were categorized under simulator factors, task factors, and individual factors.

In a recent study analyzing the cybersickness factors and the corresponding results from the previous work [32], it was

shown that the hardware/software factors explained 55.3% of the adjusted variance in a linear model estimating reports of cybersickness. Aiming to contribute to the development of effective interventions that can enhance user comfort and reduce the incidence of cybersickness, we focus this work on three VR content factors: navigation speed, scene complexity and stereoscopic rendering. Having been identified as important factors in cybersickness [10, 15, 16, 33, 34], all three can be controlled by software. In addition, tuning content variables when indicated by user biofeedback can allow to implicitly account for individual and hardware-related factors while preserving the original design intentions of the VE as much and as long as possible.

The correlation between navigation speed in a VE and the severity of cybersickness-related symptoms has been extensively investigated [35, 36]. It has been reported that an increasing navigation speed consistently heightens the severity of motion sickness but the limits of the correlation between the two was not firmly established [37]. On the other hand, the blur effect that occurs when navigation reaches high speeds was considered to reduce the cybersickness. Hu et al. [38] presented a real-time and automatic camera control approach for predicting the magnitude of the discomfort for a presented scene and camera trajectory. Based on the findings in user experiments, the method was shown to help reduce simulator sickness while maintaining the original navigation and perform better than simpler alternatives. Keshavarz et al. [33] reported that the intensity of vection, the sensation of motion solely based on visual stimuli, was connected to their speed and also affected by the crowdedness of the scene, which shows that scene content also affects cybersickness. Serrano et al. [39] proposed a motion compression strategy to alleviate vection-induced sickness, as it reduces sensory conflict. Padmanaban et al. [40] confirmed that differences in vection resulting from relative stimulus depth are correlated with motion sickness.

Increased visual realism in the VE has been shown to strengthen the sense of presence [41], while Jaeger et al. [34] pointed out that an increase in the detail level of the scene content caused a rise in SSQ scores, as well. In So et al.'s work [37], the participants experienced three different complexity levels achieved by changing the texture of the mappings. Their results also indicated a similar relationship.

Viewing stereoscopic 3D content rendered with maladjusted stereoscopic parameters cause VAC and difficulty in focusing, both of which contribute to visual discomfort leading to cybersickness [14, 42–47]. The interaxial distance of the stereoscopic camera pair has been shown to directly affect the amount of depth perceived in a VE and should be aligned with the user's interpupillary distance (IPD). Kolasinski et al. [48] investigated that cybersickness related symptoms become more severe when participant's eye separation and the spacing between the virtual cameras differs more. Kim et al. [49] presented an experimental study that can test the empirical impact of IPD misalignment on motion sickness.

The nature of cybersickness has been studied using various types of biometric feedback. Kim et al. [2] investigated the correlation between exposure duration in a VE and cybersickness using EEG, eye blink rate, heart rate, gastric tachyarrhythmia, skin conductance, and respiration rate. The results confirmed that cybersickness has a significant correlation with gastric tachyarrhythmia, eye blink rate, heart period, and EEG delta and beta waves. Another study [29] proposed a real-time cybersickness detection system with an artificial neural network (NN) whose inputs were electrocardiogram, electrooculogram, skin conductance, skin temperature, photoplethysmogram, electrogastrogram, respiration rate, and EEG signals collected from the participants exposed to a VE. The proposed system provided a narrow field of view (FOV) and voice feedback suggesting to reduce navigation speed after the detection of visual discomfort and the results indicated a significant drop in SSQ scores.

Compared to alternatives such as functional magnetic resonance imaging (fMRI), electrogastrogram (EGG) and galvanic skin resistance (GSR), EEG emerges as a promising type of biofeedback to objectively evaluate cybersickness in terms of mobility, data richness and price. Chen et al. [50] investigated the effect of motion sickness with EEG signals using a car simulator and found that alpha power attenuated in the parietal and motor areas while theta and delta band power augmented in the occipital area. Kang et al. [51] suggested a wellness platform to detect discomfort induced in a stereoscopic 3D environment by using a support vector machine (SVM) algorithm. The cybersickness was induced only by VAC and the test stimuli was exposed as random-dot stereograms to the participants through passive 3DTV. The results demonstrated that the overall average log spectra of EEG data attenuated following the increase in disparity level within binocular fusion limits of participants.

Deep learning algorithms have shown superior performance in the classification of EEG data, owing to their robust feature extraction capabilities. Kuang et al. [52] proposed a deep belief network for the classification of motor imagery tasks with raw EEG data. The classification accuracy of the proposed algorithm exhibited better performance than the SVM approach. Wilaiprasitporn et al. [53] proposed cascaded CNN and long short-term memory (CNN-LSTM) and also CNN and gated recurrent unit (CNN-GRU) networks to extract both spatial and temporal information from raw EEG data for person identification. While both methods achieved higher accuracy compared to SVM, CNN-GRU performed better than CNN-LSTM in terms of short training time and accuracy performance. Schirrmeister et al. [30] proposed neural networks in architectures with different number of convolution layers to classify motor imagery by using time series EEG signals as input. The first was a shallow network with two convolution layers that structurally modeled the filter bank common spatial pattern (FBCSP) algorithm, the winner of the brain-computer interface (BCI) competition IV 2a and 2b [54]. To extract a variety of task-related features, another deep learning architecture with five convolution layers was also proposed. The performances of the proposed models were measured by comparing them with the actual FBCSP algorithm. The results unveiled that both models provided better classification accuracy in the motor imagery task than FBCSP. Zhang et al. [55] introduced parallel and cascaded recurrent CNN architectures for intention recognition and the results demonstrated that both of the pro-

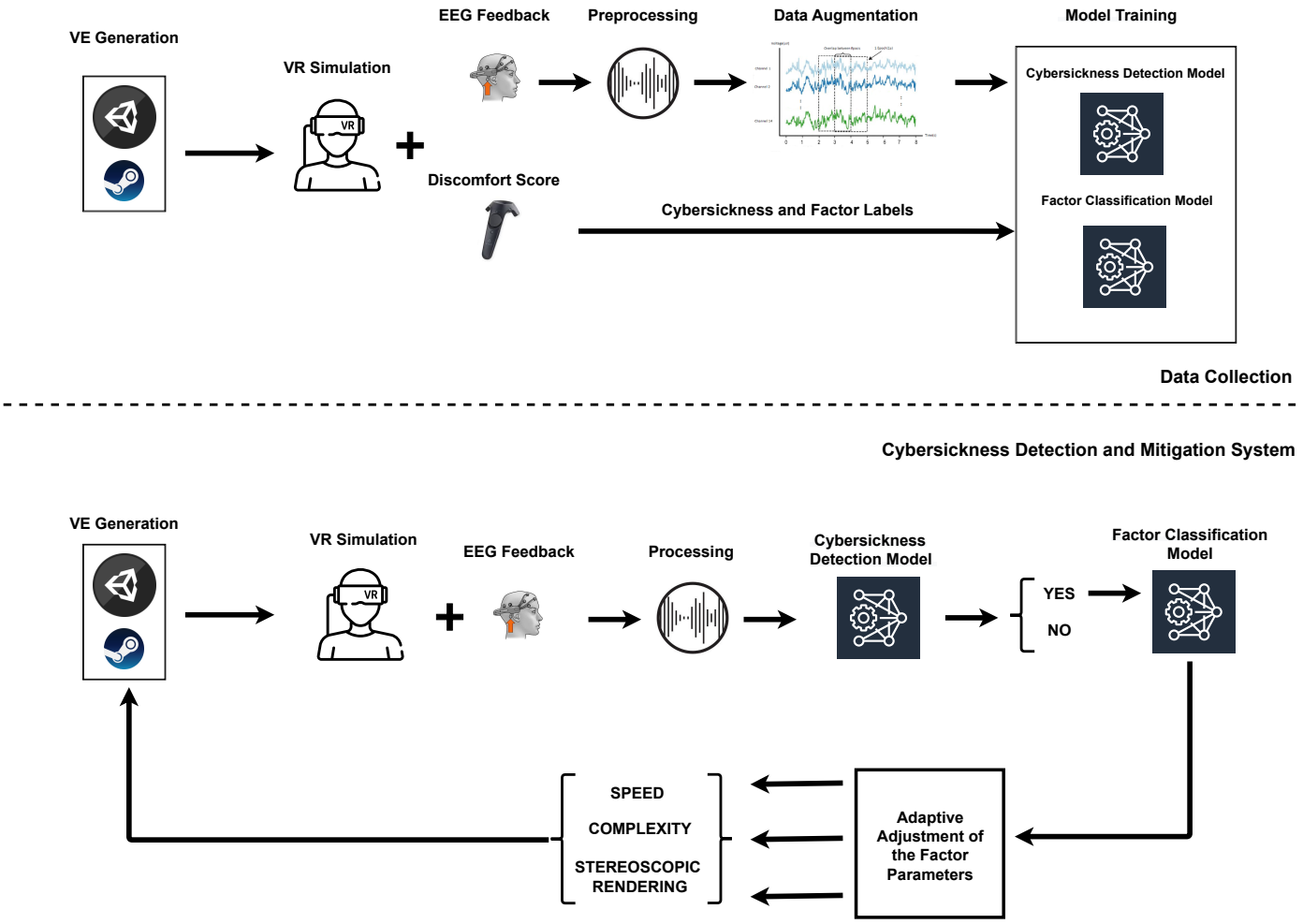

Fig. 1: Illustration of our methodology. During the data collection experiments (top half), cybersickness inducing content factors (navigation speed, scene complexity, and stereoscopic rendering) were simulated by the VE generator, in which subjects were immersed, and their responses in terms of brain activity and immediate self-reports of cybersickness severity were collected to train a two-stage shallow CNN model that first predicts the onset of cybersickness and then, in case of cybersickness, predicts the causal factor. Afterwards, the trained models are used in the CDMS loop (bottom half) to mitigate cybersickness based on the subjects' brain activity feedback by updating the VE generator simultaneously to adaptively adjust the parameters of the identified factor.

posed methods performed better than the alternatives in decoding the task-related information.

Previous approaches on mitigation [28] has not gone beyond the scope of detecting cybersickness and post-processing of the presented scene in case of detected cybersickness. The only exception is the study in which FOV is narrowed and the user is given a voice command to reduce navigation speed [29]. To our knowledge, the present study is the first work that is aimed at detecting cybersickness in relation to the three major VR content factors (speed, complexity and stereo rendering) and mitigating by adaptively tuning the parameters of the predicted factor based on the user's brain activity response.

3. Methodology

Our methodology consists of two phases, as outlined in Fig. 1. In the first phase, we collect compatible data to train the CDMS models with a formal experiment. Then, in the second phase, the trained models are used in the CDMS loop to mitigate cybersickness based on the user's brain activity feedback by adaptively adjusting the parameters of the identified factor to update the VE generator accordingly.

In this section, we first introduce the VE generator and CDMS, then outline the procedure of the data collection experiment and finally present the training performance of the CDMS models.

3.1. VE Generator

The VE Generator was developed using the Unity game engine and SteamVR plugin.

The generated VE consists of a dark, wide corridor. During the VR experience, the user is asked to watch a focal object, a blue glowing octahedron, as it moves down the corridor on a winding path and oscillates horizontally, requiring the user to shift their gaze between left and right. The focal object moves at the same speed as the trailing camera pair, which provides the user's stereoscopic view as it moves down the corridor on a straight path.

The VE generator can alter the VR experience according to the factor parameters, which can be specified by either a pa-

rameter template or CDMS. We first used the VE generator in the data collection experiment, where we employed a different template for each simulated factor, as described in Sec. 3.3. Then, we used it in the CDMS evaluation experiment (Sec. 4), where the parameters were altered dynamically by CDMS with respect to the user's cybersickness response in the CDMS session, while they followed fixed templates in the two control sessions (Fig. 7).

3.2. Cybersickness Detection and Mitigation System (CDMS)

CDMS first pre-processes the user's EEG signals, which represent the brain activity in response to the stimuli produced by the VE generator. The pre-processed EEG feedback is then fed into the first model for cybersickness detection. As long as no cybersickness is detected, CDMS will not intervene in the VE generation, i.e. the generator will continue to produce the VR experience according to a certain parameter template. However, when cybersickness is detected to have onset, the EEG feedback is also fed into the second model for factor classification so that the parameters of that factor are then gradually adjusted until CDMS determines that either the brain activity is no longer indicative of cybersickness or the limit for the adjusted parameter has been reached.

3.2.1. EEG Preprocessor

We used an Emotiv Epoc+ for EEG acquisition. Emotiv Epoc+ is a mobile EEG headset equipped with 14 saline-based electrodes and two reference electrodes [56]. It has been used in several BCI studies mostly owing to its relatively low cost and high mobility [57–60].

The EEG signals collected with the 14 electrodes were recorded at a sampling rate of 256 Hz. Bandpass filtering was applied to the 14-channel signal using a Python script to the raw data with a causal third-order Butterworth filter to include the frequency bands of theta (4 to 8Hz), alpha (8 to 12Hz), beta (12 to 25Hz), and gamma (25 or more). Delta (0.2 to 4Hz) frequency band was excluded since delta waves occur in deep sleep states, unconsciousness, or when brain activities are deficient. We did not need to apply notch filtering, because 50Hz-60Hz notch filters are implemented in the hardware internally.

3.2.2. CDMS Models

The first step in the design of a BCI is to specify the type of activity to be explored that is apt for the aimed task [61]. In this regard, the most commonly used ones are event-related-potentials (ERPs) and oscillatory activities. ERPs are time-locked voltages that are averaged over the neural responses elicited by repeated stimuli or events within the same condition. Oscillatory activities, on the other hand, are associated with power changes in specific frequency bands and they are not necessarily synchronized with the stimuli. Because cybersickness is not a transient response to a momentary stimulus but rather a cumulative effect that arises after a certain time of exposure to the stimuli, we evaluate the EEG feedback as an oscillatory activity.

While working with oscillatory activities, the actual response to be evaluated within the signal can be suppressed by noise and muscle activity-related artifacts. However, noise and artifacts elimination processes are not feasible for use in real-time applications. Artificial NN approaches can provide high generalization skills and adaptive applications thanks to their ability to handle complex data. Hence, NNs can be fed raw data directly without noise and artifact removal, and feature extraction. To this end, CNNs can be preferred over recurrent neural networks (RNNs), such as LSTMs, due to their ability to capture spatial information, computational efficiency, and reduced risk of overfitting. EEG signals are essentially time series data, but CNNs are able to capture spatial patterns by convolving over local regions of the input signal, which is useful in EEG classification tasks, where specific frequency bands are associated with different brain states or disorders. Additionally, RNNs can become computationally expensive to train for long EEG recordings, while CNNs can process local regions in parallel, making them more efficient.

CDMS uses two separate CNN models in cascade, where the first one (CDMSNet Stage1, Fig. 2) is for cybersickness detection and the second (CDMSNet Stage2, Fig. 3) is for factor classification. The architecture of the models is based on the Shallow ConvNet designed by Schirrmeister et al. [30] to detect cybersickness. The Shallow ConvNet architecture was inspired by the FBCSP algorithm [62] to classify oscillatory activities as it combines all the computational steps in a single network. Thus, all steps can be optimized jointly. The architecture was shown to have good performance on oscillatory signal classification by extracting log band-power features.

The shallow network consists of two convolutional layers: one for temporal and one for spatial convolution to deal with variations in spatial and spectral domains. The bandpass and the common spatial pattern filtering [63] steps of the FBCSP algorithm are performed as temporal and spatial convolutions in this architecture. Convolutions were utilized to generate an EEG-specific model that extracts discriminative EEG features. After two convolutional layers, batch normalization is used to standardize values in the hidden layers of the network to zero mean and unit variance. A squaring activation function, a mean pooling, and a logarithmic activation function are applied following batch normalization step to extract log band power features. The dropout technique is used to prevent over-fitting. Lastly, a dense softmax layer is utilized for classification.

We trained both models using the Adam optimization algorithm, which is a variant of stochastic gradient descent designed to work well with high-dimensional parameters with a learning rate of $6x10^{-4}$ [64]. The training was carried out by minimizing the categorical cross-entropy loss function. We ran 1000 epochs by setting the batch size to 64 and saving the model weights, which produced the highest validation accuracy. In CDMSNet Stage1, where cybersickness is detected, we set the number of filters used in the first and second convolution layers to 40 with a kernel size of 1x25 and 14x1 respectively, as shown in Fig. 2. On the other hand, in CDMSNet Stage2, where the factor is classified, we set the number of filters used in the first and second convolution layers to 50 with a kernel size of 1x25 and 14x1 respectively, as shown in Fig. 3. All models were trained in Tensorflow, using the Keras API.

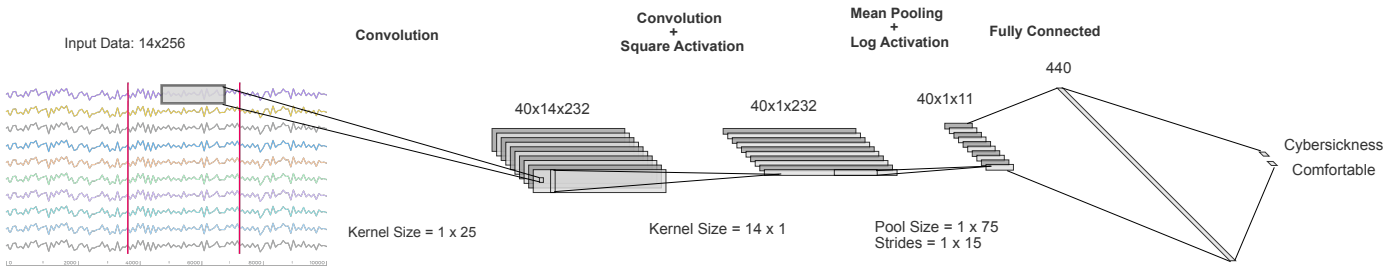

Fig. 2: Architecture of CDMSNet Stage1 used for cybersickness detection. Dimensions of inputs/feature maps and convolution/pooling kernels are indicated in the corresponding fields.

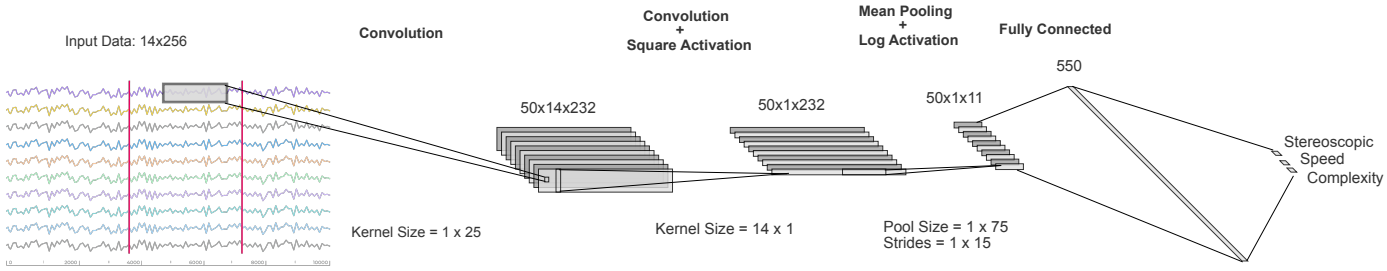

Fig. 3: Architecture of CDMSNet Stage2 used for factor classification. Convention as in Figure 2.

3.3. Data Collection

To train the CDMS models, we conducted a formal experiment to collect data and processed the recorded data as follows.

3.3.1. Participants

A total of 40 subjects volunteered to attend the training phase experiments. The data collected from five of them were excluded as they could not complete the whole set of sessions due to schedule conflicts. Besides, the data collected from two other subjects were not included as they did not report any cybersickness throughout the tests. Thus, the final sample consisted of the data collected from 33 participants (7 females and 26 males, ages 18 to 42, mean: 23.8).

The motion sickness susceptibility percentile of the sample was 29.7, which is mild and considered to be appropriate for testing, as samples skewed toward high or low susceptibility are both prone to biased results [15]. Overall, the participants had on average a low level of experience with VR (0.9 average on a 0-4 scale) and moderate video gaming habits (2.1 average on a 0-4 scale).

3.3.2. Preliminary Procedure

The experiment took place in a silent room free from external stimulus. The VE was viewed with an HTC Vive VR setup with the HMD running at 90Hz refresh rate and 1080x1200px resolution per eye.

To ascertain eligibility to participate, participants were first subjected to a stereo-blindness test using a random-dot stereogram. It was also confirmed that none of them had experienced epileptic seizures before. Then, they were informed about the general experimental procedure, cybersickness, and their right to stop the experiment at any time. They were asked to fill out the consent form and the demographic form, which included participants' gaming habits and level of VR experience to identify possible outlier data more efficiently. Also, susceptibility to motion sickness was queried using the short motion sickness susceptibility questionnaire (MSSQ) [65].

Next, they were seated and fitted with the HMD and EEG headset. The EEG electrodes were placed on the scalp according to the 10-20 system [66], as shown in Fig. A1. The Emotiv Cortex API was utilized to ensure reliable signal quality for each channel. The HMD lenses were adjusted to the participant's IPD, which was measured with a digital pupillometer.

Before testing, participants received a tutorial session, to become familiar with the VE and to learn how to report the severity of discomfort experienced during a stimulus stage. This report is referred to as the *discomfort score* (DS) and is rated on a scale from one (indicating "none") to seven (indicating "extreme") using the HTC Vive hand controller through the VR interface (without removing the HMD). During the tutorial, it was explicitly informed that only a score of 1 indicates the absence of discomfort and any feeling of discomfort should be reported with a score of 2 or higher, proportional to its severity. Accordingly, the CDMS Stage 1 model, which predicts cybersickness, is trained by labeling $DS = 1$ as no-cybersickness and $DS > 1$ as cybersickness cases.

The tutorial was continued until participants declared that they felt comfortable and proficient with the VE.

3.3.3. Testing Procedure

Following the preliminary procedure, participants proceeded to testing, in which they experienced the VE in three repeating sessions. Overall procedure of the data collection testing is given in Fig. 4.

In a test session, participants experienced each of the three VR content factors (movement speed, stereoscopic rendering

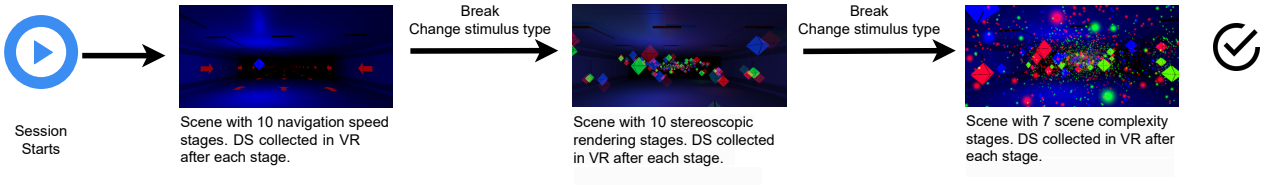

Fig. 4: Flowchart of the test procedure for a single session in the data collection experiment. Each participant experienced 3 such sessions, in which the scenes were ordered in a 3x3 Latin square design.

or scene complexity) in a separate scene of the VE. Accordingly, each factor was introduced in a predefined set of stimulus stages with breaks between them. Participants experienced ten stages of navigation speed, seven stages of scene complexity, and ten sets of stereoscopic rendering parameters, as detailed below. Each stimulus stage took 10 seconds and participants were then asked to rate their DS. After the DS was registered, the application proceeded to the next stage according to the preset order when participants pressed the designated hand controller button indicating readiness to continue.

A scene ended when all stages of the simulated factor were completed. Without removing the headsets, participants were then allowed to rest their eyes and recollect themselves for a minimum of 30 seconds while the HMD displayed a black screen.

Having finished a session by concluding all three scenes, the participants were assisted to remove the headsets. Then, they were requested to rest their eyes for at least three minutes and instructed that they could start the next session when they felt ready afterwards. Upon their indication, they were refitted with the headsets and immersed in the VE for another session.

When participants were exposed to the VE for three such sessions, the experiment was finalized. Across the sessions, the scenes were presented in a randomized order with a 3x3 Latin square design to offset possible carry-over effects between different factors. The scene details are provided below.

Navigation Speed. For the experiment, the speed of the stereoscopic camera pair was set to 10 different navigation speed stages (1.2, 2.4, 4.8, 9.6, 14.4, 19.2, 28.8, 38.4, 57.6, and 76.8 meters/sec for the consecutive stages). Particular to this scene, red arrows pointing forward were added to the surface textures in order to foster the sense of vection. Also, an emission shader was applied to these arrows to make them stand out from the focal object.

Stereoscopic Rendering Parameters. The most crucial step in generating a stereoscopic 3D image is the adjustment of the stereoscopic rendering parameters. To this end, the two principal stereoscopic rendering parameters are the convergence distance and the interaxial distance. Convergence distance defines the separation between the camera plane and the focus plane, where the image for the left/right cameras are identical, while interaxial distance simply defines the distance between the two cameras on the camera plane. By changing these two parameters from the default values held constant by the application programming interface of the HTC Vive (and other consumer grade VR-HMDs) using projection manipulations by Avan et al. [67], the generator produced stereoscopic image sequences with different disparity settings, resulting in altered perceived depth compositions.

In the experiment, only one of the stereoscopic rendering parameters was changed between consecutive stages. 10 different settings of interaxial-distance and convergence distance were tested, as given in Table 1. The copies of the focal object, in randomly assigned colors of red, green and blue, were scattered in the background to increase the number of depth cues and they were kept slightly smaller than the focal object.

Table 1: Parameters used through the stages of stereoscopic rendering scene. The bottom row gives the values used with the stages of speed and scene complexity.

Cue Stage	Interaxial Distance (cm)	Convergence Distance (m)
Stage 1	6.00	0.80
Stage 2	6.00	1.20
Stage 3	6.00	1.60
Stage 4	6.00	2.00
Stage 5	9.00	2.00
Stage 6	12.00	2.00
Stage 7	15.00	2.00
Stage 8	15.00	1.80
Stage 9	15.00	1.40
Stage 10	15.00	1.00
Other Scenes	IPD	1.50

Scene Complexity. We tested scene complexity in seven stages with increasing intensity. In the first stage, there was only the focal object in the empty corridor. The second stage had 84 copies of the focal object, which were added along the corridor edges and oscillating vertically in a sinusoidal pattern. 171 more copies were added in the third stage. These additional copies were placed in three additional lines along the corridor with increasing density towards the end. In the fourth stage, the existing copies were colored randomly in red, green, or blue. The fifth stage introduced particle emitters attached to the copies. These emitters were directed towards the central path that the camera pair followed and each generated 20 particles per second matching the color of the copy object. In the sixth stage, the particles were given HDR textures making them brighter, the emission rate was raised to 50 particles per second and also a particle force field was used to propel the particles further into the camera view. In the final stage, the particle brightness was boosted and the emission rate was further increased to 75 particles per second, thus having particles occupy most of the field of view at severe discomfort.

In the scenes simulating scene complexity and stereoscopic rendering parameters, navigation speed remained at its mini-

mum (1.2 m/s) as in the first stage of the navigation speed scene. Similarly, the stereoscopic rendering parameters were kept fixed (by setting interaxial distance to the IPD and the convergence distance to 1.5 m) in the simulation of navigation speed and scene complexity. The supplemental video material demonstrates the complete sequences of all stimulus stages for each VR content factor simulated in the data collection experiment consecutively (without the DS evaluation breaks in between).

Charts showing the per-stage average DS response for each factor throughout the data collection experiment are given in Fig. A2 of the Appendix. For a detailed analysis of the collected data in relation to the simulated stimuli and time spent in VR, we refer the reader to [68].

3.3.4. Data Processing

In order to use the 14-channel time-series EEG recordings as input in the model training, EEG data were partitioned in batches per session by factor type using the EEGLAB toolbox [69] in Matlab. Ten seconds of EEG data recorded per stimulus stage was reduced to eight seconds by trimming one-second portions from both ends. This way, possible synchronization problems and delays were eliminated. Next, the sliding window divided eight seconds of data into one-second pieces. The partitioned EEG data was labeled with corresponding factor type and DS.

To prevent data imbalance issues and ensure that the models are not overexposed to dominant classes, we applied data augmentation using overlapped partitioning of consecutive sliding windows in different ratios between label types. The data labeled with cybersickness (i.e., those with reported DS of 2 and above) were partitioned with a 50% overlap between consecutive steps of the sliding window. To train the factor classification model, the overlap between consecutive steps of the sliding window was set at 75% for partitioning the navigation speed tests' data; and 25% for partitioning the scene complexity tests' data. The stereoscopic rendering tests' data were partitioned without overlap. After partitioning, the data were labeled using the source data labels and scaled using the min-max of the current chunk.

3.4. Training Performance of the CDMS Models

The prediction accuracies of CDMSNet Stage 1 and Stage 2 were evaluated against EEGNet and DeepConvNet, both of which yield state-of-the-art decoding accuracies, especially for the motor imaginary task classification. EEGNet, a compact CNN for EEG-based BCIs, was proposed by Lawhern et al. [70]. The depthwise and separable convolutions were utilized to construct a general-purpose architecture that enables efficient feature extraction. We analyzed the performances of two different configurations of the EEGNet architecture by varying the number of filters. EEGNET4.2 has 4 temporal filters and 2 spatial filters for each temporal filter, while EEGNET8.2 has 8 temporal filters and 2 spatial filters for each temporal filter. The DeepConvNet architecture was proposed by Schirrmeister et al. [30] to be a general-purpose architecture for BCIs, unlike the Shallow ConvNet architecture, which was explicitly designed to decode oscillatory-based tasks.

For the analysis, we conducted a fivefold cross-validation. The data collected during the model training phase experiments was divided into five subsets of equal size and the models were trained in five iterations using one of the subsets (20%) as the test set and the rest as the training set in each iteration. Table 2 compares the classification accuracies of CDMSNet Stage1 and Stage2 models against the alternatives. The results show that both CDMS models outperform the alternatives, despite their shallower architecture. This is likely due to their specific design for extracting log band power features.

The performances of both models averaged over five folds are given in Table 3 in terms of precision, recall, and F-measure. The performance of CDMSNet Stage1 reached an overall accuracy of 76.26%, while CDMSNet Stage2 achieved 81.01% overall accuracy. The classification precision of each factor in CDMSNet Stage2 for each fold is given in Fig. 5c. The confusion matrices are provided in Fig. A3 of the Appendix. The results reveal that the precision of the classification on stereo rendering parameters is superior to others.

It is crucial to designate the operational frequency band effectively in the classification of oscillatory EEG signals. Chuang et al. [71] demonstrated that the reported levels of motion sickness were positively correlated with gamma and alpha bands' activation. Khaitami et al. [72] investigated the relationship between cybersickness and gamma-band deviation and found an increase in gamma deviation in the EEG signal compared to the baseline when participants were immersed in a VE. Accordingly, our CDMSNet Stage1 and CDMSNet Stage2 models were trained by including the gamma band. To better understand the gamma band contribution, the models were also trained by excluding it, and the classification performances of both cases were compared. The results revealed that the inclusion of the gamma band in the model input enables better EEG decoding accuracy, as shown in Fig. 5a and Fig. 5b.

Table 2: Overall decoding accuracies for cybersickness detection (on the left) and factor classification (on the right), computed by averaging over the accuracies obtained with 5-fold cross-validation training.

Cybersickness Detection	
EEGNET4.2	63.87%
EEGNET8.2	64.82%
Deep ConvNet	69.01%
CDMSNet Stage1	76.26%

Factor Classification	
EEGNET4.2	53.47%
EEGNET8.2	64.49%
Deep ConvNet	72.80%
CDMSNet Stage2	81.01%

Table 3: Detailed results for cybersickness detection with CDMSNet Stage1 model (on the left) and for factor classification with CDMSNet Stage2 model (on the right). The metrics were computed by averaging over all results obtained with 5-fold cross validation training.

	precision	recall	f1
No-Cybersickness	0.77	0.67	0.72
Cybersickness	0.76	0.84	0.80
Overall Accuracy	76.26%		

	precision	recall	f1
Complexity	0.77	0.70	0.73
Stereo Rendering	0.86	0.84	0.85
Speed	0.75	0.87	0.80
Overall Accuracy	81.01%		

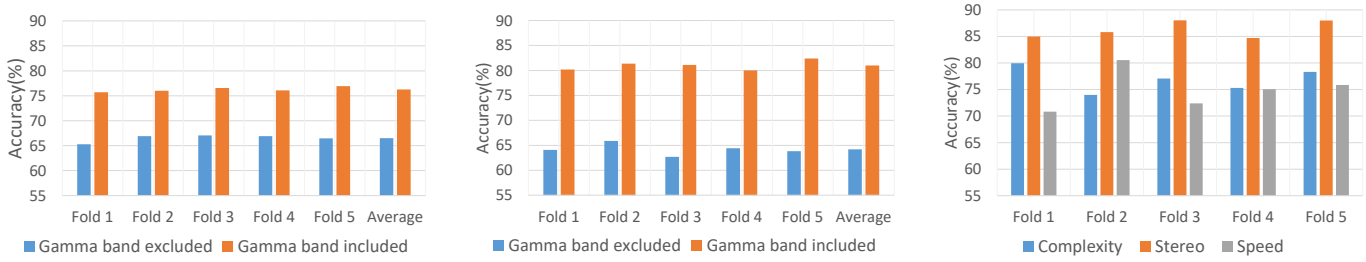

(a) (b) (c)

Fig. 5: Plots illustrating the decoding accuracies of (a) CDMSNet Stage1 and (b) CDMSNet Stage2 trained with EEG data excluding and including the gamma band (c) along with the accuracy of CDMSNet Stage2 for each class.

4. CDMS Evaluation

To evaluate the efficacy of CDMS in real-time cybersickness mitigation, we conducted an experiment consisting of one CDMS session and two control sessions (Control 1 and 2). In this section, we first describe the details of the experiment and then report and discuss the obtained results.

4.1. Participants

22 subjects, who had not participated in the data collection experiment, volunteered to take part in the CDMS evaluation experiment. One volunteer was not admitted in the experiment for failing the stereo blindness test. Another volunteer withdrew from the experiment after one session because of experiencing severe cybersickness. Hence, the tests were concluded with 20 participants (all males of ages between 22 and 33, average: 28.1). Their average MSSQ percentile was 29.1, which is close to the moderate level as the sample of the data collection experiment. On average, they had little experience with VR (0.9 average) and moderate gaming habits (1.1 average).

4.2. Procedure

The overall test procedure of the evaluation experiment is given in Fig. 6, which was preceded by the same preliminary procedure described in Sec. 3.3.2.

During testing, each participant experienced the CDMS session and the two control sessions (Control 1 and Control 2) in a randomized order. Each session lasted 105 seconds. Between the sessions, participants were asked to rest for at least three minutes and then resume when they felt ready. Participants were not informed of the CDMS mechanism or the order of the sessions.

In the Control 1 session, the parameters were changed according to the template T1 (Fig.7a), which starts with moderate speed, scene complexity, and stereoscopic rendering parameters. In T1, each parameter is gradually intensified separately. After a parameter is changed, it is returned to its initial level and then a five-second interval is observed before intensifying another parameter. The parameter levels are adjusted to fit the specific trends shown in Fig. 7a. This ensures smoother transitions and maintains a sense of presence.

In the Control 2 session, the parameters followed the template T2 (Fig.7a), which has a similar pattern to T1 at the beginning. However, in T2, once a parameter is changed to a severe level, it remains there until the end of the session, as shown in Fig. 7a. The intention was to induce a more intense level of accumulated cybersickness by introducing multiple factors that invoke cybersickness at severe levels in tandem by the end of the session.

In the CDMS session, the factor parameters adhered to the T2 template as long as CDMS did not detect cybersickness. That is, when CDMS predicted an onset of cybersickness, it also predicted the causal factor and the parameters related to that factor were gradually adjusted by CDMS. This was done by applying changes to the associated parameters in constant steps for 10 seconds, so that at the end of 10 seconds the parameters were returned to three levels before their current level on the curve specified by the T2 template. If the CDMS determined that the EEG response no longer indicated cybersickness or had already reached the limit for the set parameter, i.e., the initial value on the curve, it stopped the change before the 10 seconds were up. Overall, the changes in the factor parameters during a CDMS session reflected the curves of T2 together with the dynamic adaptive updates applied by the CDMS based on the participant's brain activity feedback.

The participants were asked to fill out the SSQ at the beginning and the end of each session. Also, they were asked to report DS after each session.

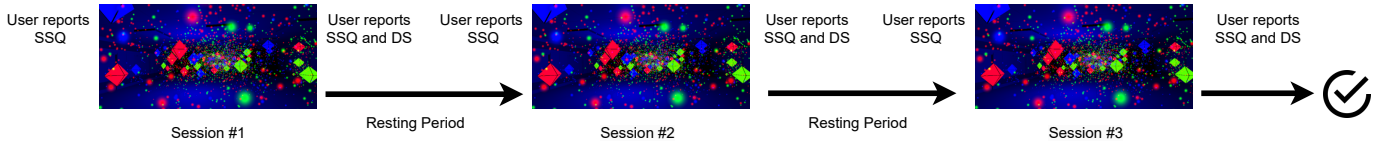

Fig. 6: Flowchart of the test procedure for a complete set of sessions in the CDMS evaluation experiment. The Control 1, Control 2, and CDMS sessions were presented in #1, #2 and #3 slots in randomized order.

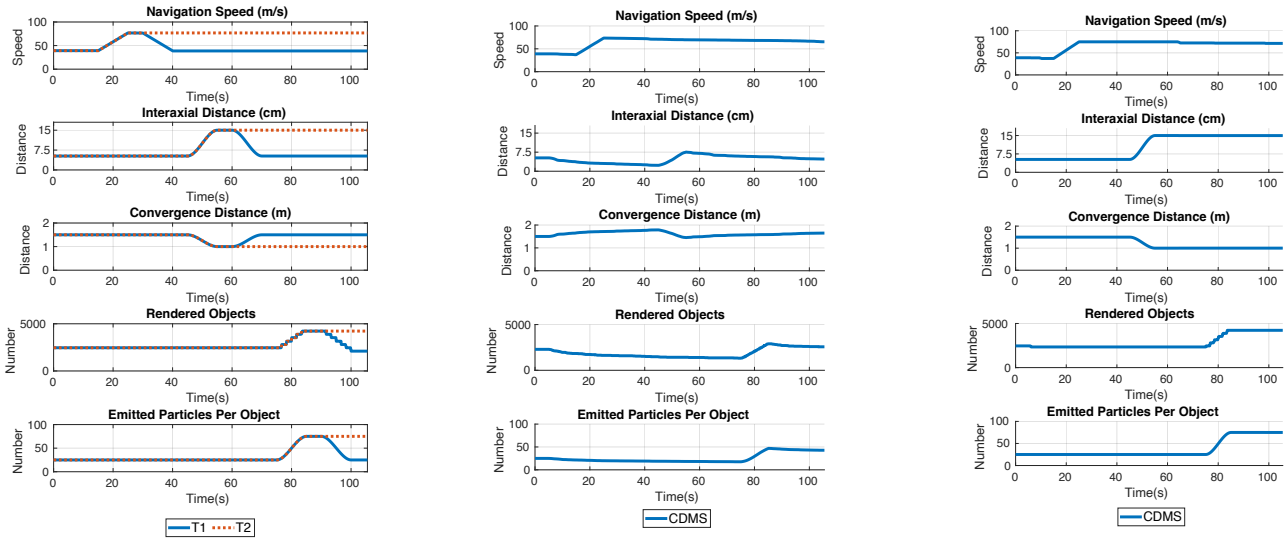

Fig. 7: Plots illustrating the changes in the factor parameters during the CDMS evaluation experiment: (a) according to the common templates in Control 1 and Control 2 sessions, and (b) as averaged over the participants who reported cybersickness in the CDMS session (c) as averaged over the participants who did not report cybersickness in the CDMS session.

4.3. Results and Discussion

The performance of CDMS was evaluated using changes in SSQ responses collected before and after each session (i.e., delta SSQ), DS responses collected after each session, and temporal changes in the factor parameters across the sessions. Three of the participants did not report cybersickness in any of the sessions, as shown in Fig. 8. Therefore, their reports were excluded from the analyses. The statistical analyses were carried out using the JASP tool [73].

Instead of considering only the post-session SSQ scores, delta SSQ scores were taken into account to eliminate the contribution of the varying levels of initial states of the participants and to isolate the effects of the experienced stimuli. An SSQ response gives out a total SSQ score (SSQ-T) in addition to three different sub-scores in nausea (SSQ-N), disorientation (SSQ-D), and oculomotor discomfort (SSQ-O). The averages for the post-session DS and the per-session delta SSQ scores are shown in Fig. 9.

While both parameter templates used in the evaluation were aimed to elicit at least a moderate level of cybersickness through the sessions, T2 was specifically designed to induce a higher level of cybersickness than T1 by driving all parameters to their most severe levels one by one and maintaining them at that level until the session's end. All indicators of reported cybersickness show that participants experienced the most intense cybersickness during the Control 2 session, as intended. It is also evident that participants experienced less cybersickness during the CDMS session than in either control session, even though the factor parameters applied in the CDMS session followed the more severe template (T2) and CDMS intervened in this template in gradual updates only during the periods when it detected cybersickness.

For further investigation, DS and delta SSQ scores were subjected to a one way repeated measures analysis of variance (RMANOVA) test to compare the differences between the levels of experienced cybersickness. RMANOVA rejected the null hypothesis for all scores, as shown in Table 4, showing that the experiences, exhibited by all considered scores, were significantly different between the three sessions. Further, a post-hoc test was applied to investigate pairwise comparisons between

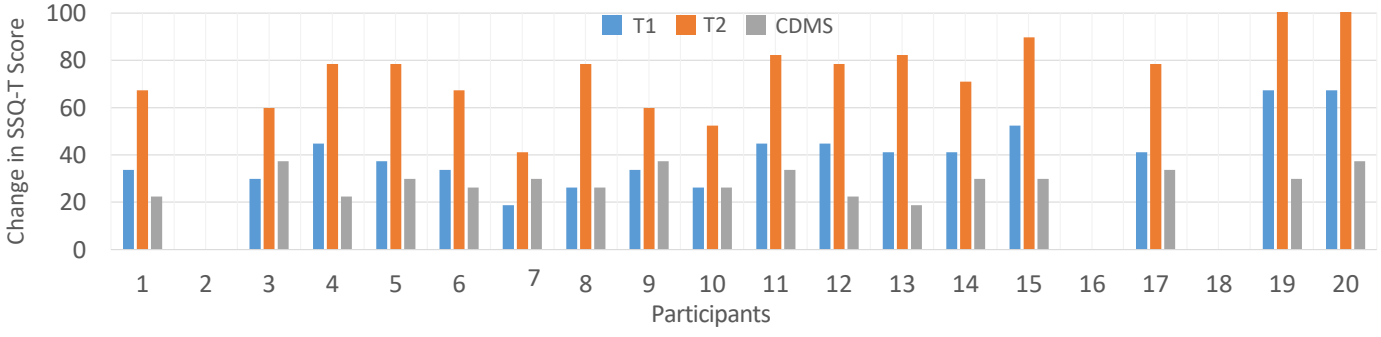

Fig. 8: Plot illustrating the individual changes in SSQ-Total scores between the beginning and the end of each session for all participants.

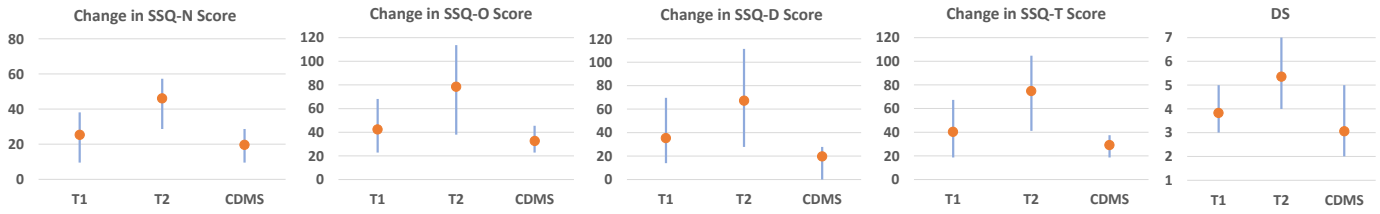

Fig. 9: Plots showing the ranges (blue bars) and the averages (orange dots) for the per-session changes in SSQ scores and end-of-session DS responses as averaged over the participants who experienced cybersickness.

the three sessions using the Holm correction for all scores. The pairwise comparison revealed that there is a significant difference between the Control 1, the Control 2, and the CDMS sessions in all paired samples of SSQ-T, SSQ-N, SSQ-O, SSQ-D and DS responses. The results are given in Table A1 of the Appendix. It is seen that the sessions had a statistically significant effect on cybersickness, suggesting that the experimental design, including the procedurally generated VE, were properly suited for our goals.

Participants P2, P16 and P18 (Fig. 8), who reported all SSQ responses as 0 and all DS responses as 1 out of 7 were considered to have reported no cybersickness. The temporal changes in factor parameters averaged across the records of these participants in the CDMS session are shown in Fig. 7c. The curves demonstrate minimal intervention by CDMS, as evidenced by the similarity of the curves to the T2 template. That is, CDMS made only minor updates for these participants, which did not significantly alter the parameters. This suggests that CDMS can sustain the intended VR experience, including presence and immersion, by avoiding false positives while maintaining sufficient performance.

In contrast, Fig. 7b shows the temporal changes in the parameters during the CDMS session, averaged over the records of the participants who reported cybersickness. The curves highlight the differences in comparison to T2 resulting from CDMS interventions due to detected cybersickness. The data shows that CDMS intervened the most with the stereoscopic rendering parameters and the least with navigation speed. This suggests that the experienced cybersickness was primarily caused by the stereoscopic rendering parameters and least by navigation speed. It is also seen that the CDMS interventions prevented the complexity and stereoscopic rendering parameters from reaching severe levels by the session's end, instead maintaining them at moderate levels. Navigation speed was minimally intervened with until it reached high levels, at which point it was gradually reduced based on the received brain activity feedback. Altogether, the average curves obtained support the prior finding that the CDMS session resulted in the lowest overall cybersickness.

Table 4: Average changes in the SSQ subscores and DS per session along with the RMANOVA test results.

	Control 1 (M ± SD)	Control 2 (M ± SD)	CDMS (M ± SD)	Significance
Change in SSQ-N Score	25.2 ± 8.8	46.0 ± 8.4	19.6 ± 6.2	$F_{2,32} = 125.209$ $p < .001$
Change is SSQ-O Score	42.3 ± 21.2	78.4 ± 18.7	32.5 ± 6.9	$F_{2,32} = 82.447$ $p < .001$
Change in SSQ-D Score	35.2 ± 17.1	67.1 ± 21.5	19.6 ± 9.9	$F_{2,32} = 56.485$ $p < .001$
Change in SSQ-T Score	40.2 ± 13.1	74.8 ± 16.1	29.0 ± 5.6	$F_{2,32} = 111.331$ $p < .001$
Discomfort Score	3.8 ± 0.8	5.3 ± 1.1	3.0 ± 0.7	$F_{2,32} = 97.567$ $p < .001$

The individual parameter curves experienced by the participants during the CDMS session are provided in Fig. A4 and A5 of the Appendix, for those who reported cybersickness and those who did not, respectively.

Finally, we conducted a correlation analysis to further evaluate the impact of the CDMS on the factor parameters. The parameters recorded during the CDMS session were averaged for each participant and tested for correlation with their cybersickness reports (the delta SSQ-T score and the average of the DS responses) for the CDMS session and their susceptibility to motion sickness (MSSQ percentile). The analysis also examined the correlations between the two self-reported outcomes and susceptibility to motion sickness. The results are illustrated in Fig. 10. A low average for the camera convergence distance or a high average for any other factor parameter indicates minimal or no intervention by CDMS in that particular parameter. Such that, participants with lower SSQ-T change tend to have higher averages in the factor parameters (and lower for the converge distance), as CDMS observed less cybersickness and made fewer interventions to produce milder parameters during their sessions. This finding aligns with the observation that changes in SSQ-T are positively correlated with convergence distance and negatively correlated with interaxial distance, particle rate, and the number of rendered objects. Besides, there is a low correlation between the delta SSQ-T score and navigation speed, which is consistent with the results of the data collection experiment, indicating that the participants experienced less cybersickness related to speed. The strong negative correlation between the MSSQ percentile and recorded navigation speed suggests that MSSQ could serve as a predictor of the navigation speed -related cybersickness experienced in a VE. Furthermore, there is a strong positive correlation between the delta SSQ-T and DS, which measures immediate discomfort. This implies that single-item queries, by which the user is interrupted minimally, can be an efficient measure for assessing cybersickness severity.

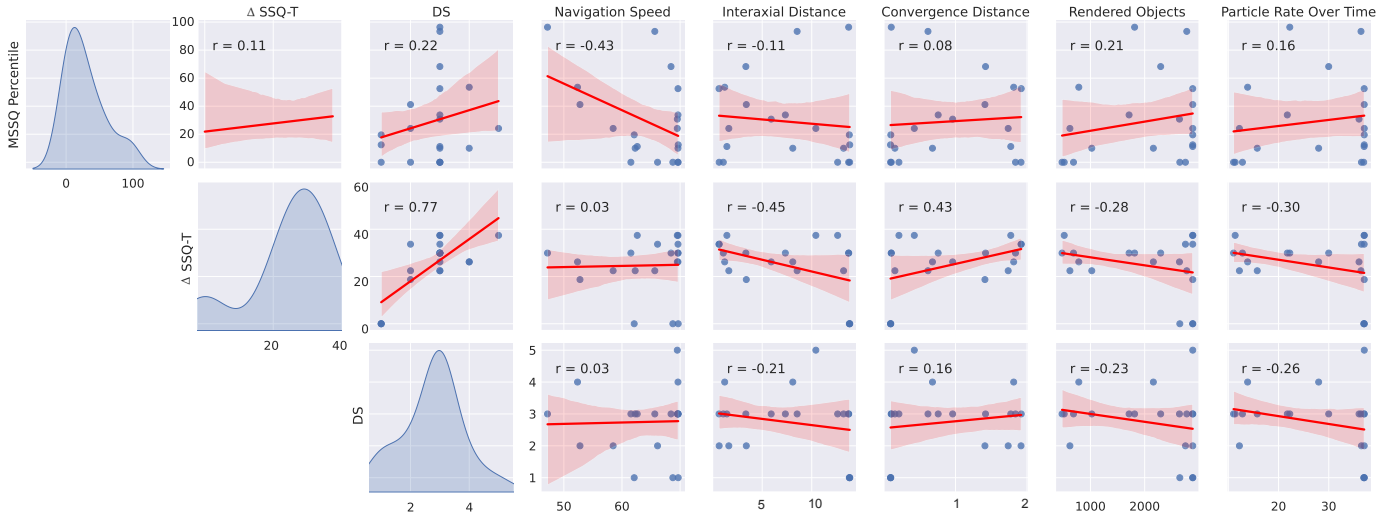

Fig. 10: Plots showing the correlations between the MSSQ percentile, delta SSQ-T score, DS, and the averages of the factor parameters over the CDMS session.

5. Limitations and Future Work

The brain feedback was analyzed in terms of oscillatory activities, as per the restrictions in Section 3.2.2. Although this scheme yielded rich data on the vision-related brain response to simulated VR stimuli, oscillatory activities are vulnerable to noise and other artifacts, which can limit their accuracy. Furthermore, the EEG data collected during free-viewing was subject to additional artifacts caused by participants' head and eye movements. To address these challenges, a two-stage convolutional network architecture was used. However, it is possible that their influence was not completely remedied.

The experimental design was subject to certain limitations, as well. During data collection, while the order of the scenes was counterbalanced, the stages within each scene were fixed. This aspect was based on previous work on cybersickness prediction [74, 75], wherein cybersickness reports were collected at frequent intervals while the same videos (i.e., lengthy sequences of exactly the same stimuli) were presented to all participants. Similarly, there have been other studies in which cybersickness reports were collected using a series of short-term stimuli [76–78]. As evidenced by participants' responses, our 10-second stages were effective in inducing cybersickness. However, the presentation of stages in a fixed order can be regarded as restricting. Furthermore, the VE generator is highly customized for CDMS, resulting in a more abstract environment than those encountered in typical VR applications. Nevertheless, the VE was effective in allowing us to capture the effects of each simulated factor in isolation and to mitigate cybersickness by automatically adjusting the factor parameters based on the CDMS feedback. It should be noted, however, that some scene elements used in the navigation speed trials to induce optic flow, such as the red arrows, may have impeded the intended outcome at higher speeds by inducing wagon-wheel illusions. These factors may have reduced the perceived speed of self-motion and contributed to the relatively smaller effect of speed on the experienced cybersickness.

Our study provides a foundation for future research on cybersickness mitigation by experimenting with cybersickness factors in conjunction. To further our efforts, future work would benefit from using more typical VEs with experimental designs that are less susceptible to order effects. Once the tuning of the investigated factor content parameters is achieved in the targeted VEs, extending our approach to them will be straightforward. Using a subset of channels by analyzing the effects of EEG feedback from different regions of the scalp on online mitigation performance could also be a valuable direction for future research [68, 79].

A final limitation to note is the sample demographics. Although the samples for the data collection and CDMS evaluation experiments had similar age statistics, MSSQ percentiles, and video gaming habits, our CDMS evaluation experiment only included male participants. Conducting future studies with larger and more balanced samples would provide a broader understanding of cybersickness in relation to the factors under consideration.

6. Conclusion

In this study, we proposed an EEG-based system called CDMS for simultaneous detection and mitigation of the cybersickness experienced by VR-HMD users. We conducted our study by focusing on navigation speed, scene complexity, and stereoscopic rendering. By varying these three factors, which are among the major content factors of cybersickness, we induced cybersickness in the data collection experiment. A supplementary video demonstrating a complete run of the three scenes used in this experiment is provided. The EEG data collected from the participants was labeled with their corresponding scores of experienced cybersickness. After applying data augmentation, the finalized dataset was used to train a two-stage shallow CNN model for detecting cybersickness and classifying the causal factor. The models reached decoding accuracies of 76.26% and 81.01%, respectively, outperforming both EEGNet and the DeepConvNet architectures. The training results also showed that the gamma band's inclusion increases accuracy by a considerable margin.

To assess the online performance of CDMS, an evaluation study was conducted with a different group of participants. The participants were exposed to two control sessions in addition to the session in which CDMS was used. The results showed that CDMS was successful in mitigating cybersickness, despite the challenges posed by the cross-subject variability in the experiment. The outcomes also suggest that CDMS can help maintain immersion and presence by providing non-invasive cybersickness mitigation with sufficient performance.

We have made all user feedback, including processed EEG data and self-reports of experienced cybersickness, collected from both the data collection experiment and the CDMS evaluation experiment, available on the paper website along with the code used to process the data.

To our knowledge, this is the first attempt to mitigate cybersickness by distinguishing for multiple content factors conjointly and tuning the parameters of the predicted causal factor in real-time based on the user's biofeedback. However, as indicated in the previous section, our study was realized with certain limitations. Future work extending our approach by addressing these limitations can help to achieve further user comfort by improved cybersickness mitigation and to provide prolonged VR-HMD experiences.

Declarations

Data Availability. The processed data used in this work is available at the paper website.

Code availability. The code used to process the data is available at the paper website.

Funding. This work was supported by the Scientific and Technical Research Council of Turkey (TUBITAK, project grant number 116E280).

Conflicts of interest/Competing interests. The authors declare that they have no known competing financial interests or personal relationships that could have appeared to influence the work reported in this paper.

Ethics approval. This study has been approved by Hacettepe University Ethics Board.

Consent to participate. Written informed consent was obtained from all individuals participated in this study.

Consent for publication. The participants consented to the publication of their collected data without identifying information.

Acknowledgements

We thank Alper Özkan for his contributions to the initial version of the VE generator component and the data collection experiment. We also wish to express gratitude to all those who voluntarily participated in our experiments, for their time and involvement.

References

[1] Y.C. Chen, X. Dong, J. Hagstrom, T. Stoffregen, Control of a virtual ambulation influences body movement and motion sickness, BIO Web of Conferences 1 (2011) 00016.

[2] Y. Kim, H. Kim, E. Kim, H. Ko, H.T. Kim, Characteristic changes in the physiological components of cybersickness, Psychophysiology 42 (2005) 616–25.

[3] P. DiZio, J.R. Lackner, Circumventing side effects of immersive virtual environments, Advances in human factors/ergonomics 21 (1997) 893–896.

[4] M. Mon-Williams, J. Wann, S. Rushton, Design factors in stereoscopic virtual-reality displays, Journal of The Society for Information Display - J SOC INF DISP 3 (1995).

[5] U. Celikcan, Eğitimde ve tıpta sanal gerçeklik uygulamaları: Geçmişten geleceğe uzanan bir İnceleme, 2022. doi:10.24012/dumf.1097748.

[6] P. Bockelman, D. Lingum, Factors of cybersickness, in: International Conference on Human-Computer Interaction, Springer, 2017, pp. 3–8.

[7] J.E. Bos, W. Bles, E.L. Groen, A theory on visually induced motion sickness, Displays 29 (2008) 47–57. Health and Safety Aspects of Visual Displays.

[8] J.T. Reason, J.J. Brand, Motion sickness., Academic press, 1975.

[9] J. Bos, Visually induced and modulated, but vestibularly caused motion sickness. 4th int, in: Symp. on Visual IMage Safety, VIMS2013, Stratford-upon-Avon, UK, 2013, pp. 3–4.

[10] B.D. Lawson, P. Proietti, O. Burov, P. Sjölund, T. Rodabaugh, R. Kirollos, M. Bloch, –factors impacting cybersickness, NATO STO Technical Report: Guidelines for Mitigating Cybersickness in Virtual Reality Systems (2022).

[11] M. Allue, A. Serrano, M.G. Bedia, B. Masia, Crossmodal perception in immersive environments., CEIG 16 (2016) 1–7.

[12] D.M. Hoffman, A.R. Girshick, K. Akeley, M.S. Banks, Vergence–accommodation conflicts hinder visual performance and cause visual fatigue, Journal of Vision 8 (2008) 33–33.

[13] A. Sherstyuk, A. Dey, C. Sandor, A. State, Dynamic eye convergence for head-mounted displays improves user performance in virtual environments, in: Proceedings of the ACM SIGGRAPH Symposium on Interactive 3D Graphics and Games, 2012, pp. 23–30.

[14] T. Shibata, J. Kim, D.M. Hoffman, M.S. Banks, The zone of comfort: Predicting visual discomfort with stereo displays, Journal of vision 11 (2011) 11–11.

[15] L. Rebenitsch, C. Owen, Review on cybersickness in applications and visual displays, Virtual Reality 20 (2016) 101–125.

[16] IEEE Standard for Head-Mounted Display (HMD)-Based Virtual Reality(VR) Sickness Reduction Technology, IEEE, 2021. doi:10.1109/IEEESTD.2021.9416950.

[17] R.S. Kennedy, N.E. Lane, K.S. Berbaum, M.G. Lilienthal, Simulator sickness questionnaire: An enhanced method for quantifying simulator sickness, The international journal of aviation psychology 3 (1993) 203–220.

[18] G.E. Riccio, T.A. Stoffregen, An ecological theory of motion sickness and postural instability, Ecological psychology 3 (1991) 195–240.

[19] D. Gower, M. Lilienthal, R. Kennedy, J. Fowlkes, Simulator sickness in us army and navy fixed-and rotary-wing flight simulators, in: AGARD Conference Proceedings 433. Motion Cues in Flight Simulation and Simulator Induced Sickness, 1988.

[20] M.S. Dennison, M. D'Zmura, Cybersickness without the wobble: Experimental results speak against postural instability theory, Applied ergonomics 58 (2017) 215–223.

[21] J.E. Bos, Nuancing the relationship between motion sickness and postural stability, Displays 32 (2011) 189–193.

[22] E. Chang, M. Billinghurst, B. Yoo, Brain activity during cybersickness: a scoping review, Virtual Reality 27 (2023) 1–25.

[23] H. Yamamura, H. Baldauf, K. Kunze, Hemodynamicvr-adapting the user's field of view during virtual reality locomotion tasks to reduce cybersickness using wearable functional near-infrared spectroscopy, in: Proceedings of the Augmented Humans International Conference 2021, 2021, pp. 223–227.

[24] K.M.T. Pöhlmann, H.A. Maior, J. Föcker, L. O'Hare, A. Parke, A. Ladowska, P. Dickinson, I think i don't feel sick: Exploring the relationship between cognitive demand and cybersickness in virtual reality using fnirs, in: Proceedings of the 2023 CHI Conference on Human Factors in Computing Systems, 2023, pp. 1–16.

[25] Y. Kim, H. Kim, E. Kim, H. Ko, H.T. Kim, Characteristic changes in the physiological components of cybersickness, Psychophysiology 42 (2005) 616–25.

[26] E. Krokos, A. Varshney, Quantifying vr cybersickness using eeg, Virtual

Reality 26 (2022) 1–13.
[27] J. Frey, L. Pommereau, F. Lotte, M. Hachet, Assessing the zone of comfort in stereoscopic displays using eeg, in: CHI '14 Extended Abstracts on Human Factors in Computing Systems, CHI EA '14, Association for Computing Machinery, New York, NY, USA, 2014, p. 2041–2046. URL: https://doi.org/10.1145/2559206.2581191. doi:10.1145/2559206.2581191.
[28] R. Islam, S. Ang, J. Quarles, Cybersense: A closed-loop framework to detect cybersickness severity and adaptively apply reduction techniques, in: 2021 IEEE Conference on Virtual Reality and 3D User Interfaces Abstracts and Workshops (VRW), IEEE, 2021, pp. 148–155.
[29] Y.Y. Kim, E.N. Kim, M.J. Park, K.S. Park, H.D. Ko, H.T. Kim, The application of biosignal feedback for reducing cybersickness from exposure to a virtual environment, Presence: Teleoperators and Virtual Environments 17 (2008) 1–16.
[30] R.T. Schirrmeister, J.T. Springenberg, L.D.J. Fiederer, M. Glasstetter, K. Eggensperger, M. Tangermann, F. Hutter, W. Burgard, T. Ball, Deep learning with convolutional neural networks for eeg decoding and visualization, Human Brain Mapping 38 (2017) 5391–5420.
[31] E.M. Kolasinski, Simulator Sickness in Virtual Environments., Technical Report, Army research Inst for the behavioral and social sciences Alexandria VA, 1995.
[32] L. Rebenitsch, C. Owen, Estimating cybersickness from virtual reality applications, Virtual Reality 25 (2021) 165–174.
[33] B. Keshavarz, A.E. Philipp-Muller, W. Hemmerich, B.E. Riecke, J.L. Campos, The effect of visual motion stimulus characteristics on vection and visually induced motion sickness, Displays 58 (2019) 71–81.
[34] B.K. Jaeger, R.R. Mourant, Comparison of simulator sickness using static and dynamic walking simulators, Proceedings of the Human Factors and Ergonomics Society Annual Meeting 45 (2001) 1896–1900.
[35] A. Ozkan, U. Celikcan, The relationship between cybersickness and eye-activity in response to varying speed, scene complexity and stereoscopic vr parameters, International Journal of Human-Computer Studies 176 (2023) 103039.
[36] U. Celikcan, Detection and mitigation of cybersickness via eeg-based visual comfort improvement, in: 2019 3rd international symposium on multidisciplinary studies and innovative technologies (ISMSIT), IEEE, 2019, pp. 1–4.
[37] R.H.Y. So, A. Ho, W.T. Lo, A metric to quantify virtual scene movement for the study of cybersickness: Definition, implementation, and verification, Presence 10 (2001) 193–215.
[38] P. Hu, Q. Sun, P. Didyk, L.Y. Wei, A. Kaufman, Reducing simulator sickness with perceptual camera control, ACM Transactions on Graphics 38 (2019).
[39] A. Serrano, D. Martin, D. Gutierrez, K. Myszkowski, B. Masia, Imperceptible manipulation of lateral camera motion for improved virtual reality applications, ACM Trans. Graph. 39 (2020).
[40] N. Padmanaban, T. Ruban, V. Sitzmann, A.M. Norcia, G. Wetzstein, Towards a machine-learning approach for sickness prediction in 360 stereoscopic videos, IEEE Transactions on Visualization and Computer Graphics 24 (2018) 1594–1603.
[41] R. Welch, T. Blackmon, A. Liu, B. Mellers, L. Stark, The effects of pictorial realism, Teleoperators and Virtual Environments - Presence (1996).
[42] Z.M. Elias, U.M. Batumalai, A.N.H. Azmi, Virtual reality games on accommodation and convergence, Applied ergonomics 81 (2019) 102879.
[43] M. Lambooij, W. IJsselsteijn, M. Fortuin, I. Heynderickx, et al., Visual discomfort and visual fatigue of stereoscopic displays: a review, Journal of imaging science and technology 53 (2009) 30201–1.
[44] D.M. Hoffman, M.S. Banks, Focus information is used to interpret binocular images, Journal of vision 10 (2010) 13–13.
[45] A. Szpak, S.C. Michalski, D. Saredakis, C.S. Chen, T. Loetscher, Beyond feeling sick: The visual and cognitive aftereffects of virtual reality, IEEE Access 7 (2019) 130883–130892.
[46] Y. Zheng, X. Zhao, L. Yao, The assessment of the visual discomfort caused by vergence-accommodation conflicts based on eeg, Journal of the Society for Information Display (2019).
[47] B. Zou, Y. Liu, M. Guo, Y. Wang, Eeg-based assessment of stereoscopic 3d visual fatigue caused by vergence-accommodation conflict, Journal of Display Technology 11 (2015) 1076–1083.
[48] E. Kolasinski, R. Gilson, Simulator sickness and related findings in a virtual environment, Proceedings of the Human Factors and Ergonomics Society Annual Meeting 42 (1998) 1511–1515.
[49] H. Kim, J.H. Park, Effects of simulator sickness and emotional responses when inter-pupillary distance misalignment occurs, in: W. Karwowski, T. Ahram (Eds.), Intelligent Human Systems Integration 2019, Springer International Publishing, Cham, 2019, pp. 442–447.
[50] Y.C. Chen, J.R. Duann, S.W. Chuang, C.L. Lin, L.W. Ko, T.P. Jung, C.T. Lin, Spatial and temporal eeg dynamics of motion sickness, NeuroImage 49 (2010) 2862–2870.
[51] M.K. Kang, H. Cho, H.M. Park, S.C. Jun, K.J. Yoon, A wellness platform for stereoscopic 3d video systems using eeg-based visual discomfort evaluation technology, Applied ergonomics 62 (2017) 158–167.
[52] X. An, D. Kuang, X. Guo, Y. Zhao, L. He, A deep learning method for classification of eeg data based on motor imagery, in: Intelligent Computing in Bioinformatics: 10th International Conference, ICIC 2014, Taiyuan, China, August 3-6, 2014. Proceedings 10, Springer, 2014, pp. 203–210.
[53] T. Wilaiprasitporn, A. Ditthapron, K. Matchaparn, T. Tongbuasirilai, N. Banluesombatkul, E. Chuangsuwanich, Affective eeg-based person identification using the deep learning approach, IEEE Transactions on Cognitive and Developmental Systems (2019) 1–1.
[54] K.K. Ang, Z.Y. Chin, C. Wang, C. Guan, H. Zhang, Filter bank common spatial pattern algorithm on bci competition iv datasets 2a and 2b, Frontiers in Neuroscience 6 (2012) 39.
[55] D. Zhang, L. Yao, X. Zhang, S. Wang, W. Chen, R. Boots, Eeg-based intention recognition from spatio-temporal representations via cascade and parallel convolutional recurrent neural networks, 2017. arXiv:1708.06578.
[56] Emotiv, Emotiv epoc+, https://www.emotiv.com/epoc/, 2023. Accessed: 2024-01-07.
[57] B. Šumak, M. Špindler, M. Pušnik, Design and development of contactless interaction with computers based on the emotiv epoc+ device, in: 2017 40th International Convention on Information and Communication Technology, Electronics and Microelectronics (MIPRO), IEEE, 2017, pp. 576–581.
[58] R. Sanchez-Reolid, M.C. Martínez-Sáez, B. García-Martínez, L. Fernández-Aguilar, L. Ros, J.M. Latorre, A. Fernández-Caballero, Emotion classification from eeg with a low-cost bci versus a high-end equipment, International journal of neural systems 32 (2022) 2250041.
[59] I.A. Fouad, A robust and reliable online p300-based bci system using emotiv epoc+ headset, Journal of Medical Engineering & Technology 45 (2021) 94–114.
[60] Y. Daşdemir, Cognitive investigation on the effect of augmented reality-based reading on emotion classification performance: A new dataset, Biomedical Signal Processing and Control 78 (2022) 103942.
[61] J.M. Schneider, M.J. Maguire, Identifying the relationship between oscillatory dynamics and event-related responses, International Journal of Psychophysiology 133 (2018) 182–192.
[62] Kai Keng Ang, Zheng Yang Chin, Haihong Zhang, Cuntai Guan, Filter bank common spatial pattern (fbcsp) in brain-computer interface, in: 2008 IEEE International Joint Conference on Neural Networks (IEEE World Congress on Computational Intelligence), 2008, pp. 2390–2397. doi:10.1109/IJCNN.2008.4634130.
[63] H. Ramoser, J. Muller-Gerking, G. Pfurtscheller, Optimal spatial filtering of single trial eeg during imagined hand movement, IEEE Transactions on Rehabilitation Engineering 8 (2000) 441–446.
[64] D.P. Kingma, J. Ba, Adam: A method for stochastic optimization, 2014. arXiv:1412.6980.
[65] J.F. Golding, Predicting individual differences in motion sickness susceptibility by questionnaire, Personality and Individual differences 41 (2006) 237–248.
[66] R.W. Homan, J. Herman, P. Purdy, Cerebral location of international 10–20 system electrode placement, Electroencephalography and clinical neurophysiology 66 (1987) 376–382.
[67] E. Avan, T.K. Capin, H. Gurcay, U. Celikcan, Enhancing vr experience with rbf interpolation based dynamic tuning of stereoscopic rendering, Computers & Graphics 102 (2022) 390–401.
[68] A. Ozkan, U. Uyan, U. Celikcan, Effects of speed, complexity and stereoscopic vr cues on cybersickness examined via eeg and self-reported measures, Displays 78 (2023) 102415.
[69] A. Delorme, S. Makeig, Eeglab: an open source toolbox for analysis of single-trial eeg dynamics including independent component analysis, Journal of neuroscience methods 134 (2004) 9–21.
[70] V.J. Lawhern, A.J. Solon, N.R. Waytowich, S.M. Gordon, C.P. Hung, B.J.

Lance, Eegnet: a compact convolutional neural network for eeg-based brain–computer interfaces, Journal of Neural Engineering 15 (2018) 056013.
[71] S.W. Chuang, C.H. Chuang, Y.H. Yu, J.T. King, C.T. Lin, Eeg alpha and gamma modulators mediate motion sickness-related spectral responses, International journal of neural systems 26 (2016) 1650007.
[72] Khaitami, A.D. Wibawa, S. Mardi, S. Nugroho, A.Z. Khoirunnisaa, Eeg visualization for cybersickness detection during playing 3d video games, in: 2019 International Seminar on Intelligent Technology and Its Applications (ISITIA), 2019, pp. 325–330. doi:10.1109/ISITIA.2019.8937083.
[73] JASP Team, JASP (Version 0.11.1)[Computer software], 2019. URL: https://jasp-stats.org/.
[74] R. Islam, K. Desai, J. Quarles, Cybersickness prediction from integrated hmd's sensors: A multimodal deep fusion approach using eye-tracking and head-tracking data, in: 2021 IEEE international symposium on mixed and augmented reality (ISMAR), IEEE, 2021, pp. 31–40.
[75] R. Islam, Y. Lee, M. Jaloli, I. Muhammad, D. Zhu, P. Rad, Y. Huang, J. Quarles, Automatic detection and prediction of cybersickness severity using deep neural networks from user's physiological signals, in: 2020 IEEE international symposium on mixed and augmented reality (ISMAR), IEEE, 2020, pp. 400–411.
[76] L. Terenzi, P. Zaal, Rotational and translational velocity and acceleration thresholds for the onset of cybersickness in virtual reality, in: AIAA Scitech 2020 Forum, 2020, p. 0171.
[77] K.M.T. Pöhlmann, J. Föcker, P. Dickinson, A. Parke, L. O'Hare, The effect of motion direction and eccentricity on vection, vr sickness and head movements in virtual reality, Multisensory Research 34 (2021) 623–662.
[78] K.M.T. Pöhlmann, J. Föcker, P. Dickinson, A. Parke, L. O'Hare, The relationship between vection, cybersickness and head movements elicited by illusory motion in virtual reality, Displays 71 (2022) 102111.
[79] G. Li, M. McGill, S. Brewster, C.P. Chen, J.A. Anguera, A. Gazzaley, F. Pollick, Multimodal biosensing for vestibular network-based cybersickness detection, IEEE Journal of Biomedical and Health Informatics 26 (2021) 2469–2480.

Appendix

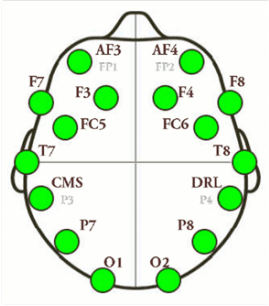

Fig. A1: Electrode placement locations of the EEG headset on the scalp. The upper part shows the front of the head. CMS/DRL references are located at P3/P4. Adapted from [56].

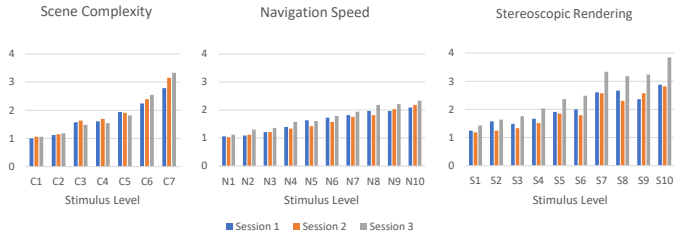

Fig. A2: Averages of the DS reports for each factor type throughout the data collection experiment.

Table A1: Holm post-hoc test results.

Measure	Test Pair		t	p_{holm}
SSQ-N	T1	T2	-11.824	< 0.001
	T1	CDMS	3.196	0.003
	T2	CDMS	15.020	< 0.001
SSQ-O	T1	T2	-9.588	< 0.001
	T1	CDMS	2.604	0.014
	T2	CDMS	12.192	< 0.001
SSQ-D	T1	T2	-7.009	< 0.001
	T1	CDMS	3.415	0.002
	T2	CDMS	10.424	< 0.001
SSQ-T	T1	T2	-10.805	< 0.001
	T1	CDMS	3.510	< 0.001
	T2	CDMS	14.315	< 0.001
DS	T1	T2	-9.145	< 0.001
	T1	CDMS	4.572	< 0.001
	T2	CDMS	13.717	< 0.001

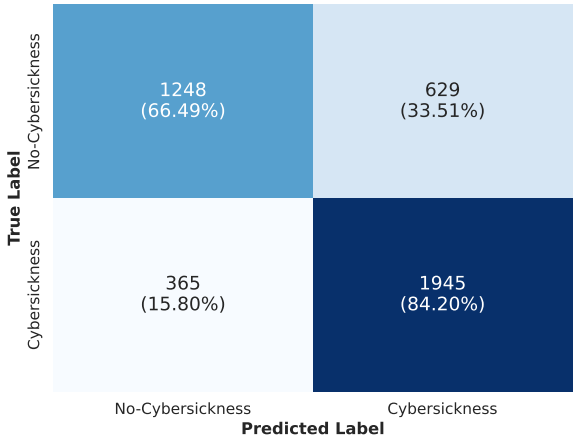

(a)

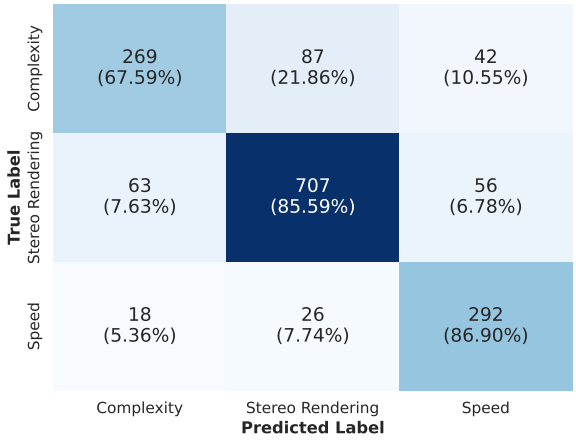

(b)

Fig. A3: Confusion matrices for a) CDMSNet Stage 1 and b) CDMSNet Stage 2.

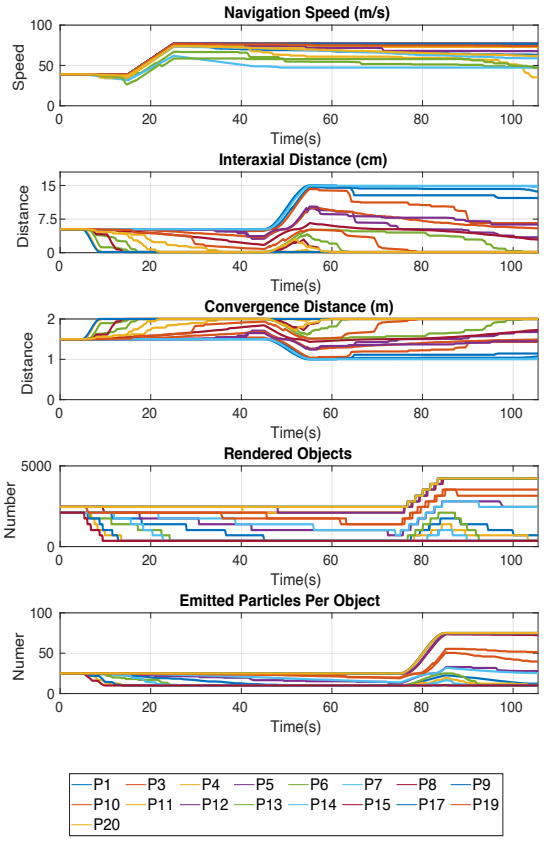

Fig. A4: Plots showing the individual curves of the factor parameters for the participants who experienced cybersickness.

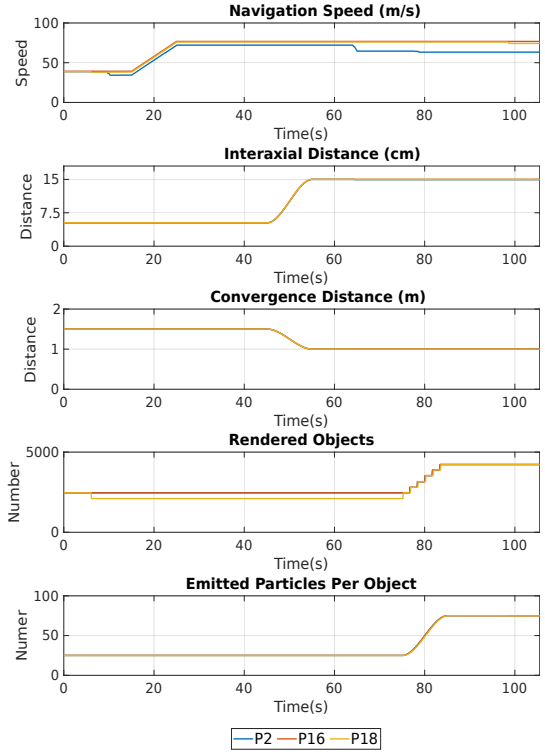

Fig. A5: Plots showing the individual curves of the factor parameters for the participants who did not experience cybersickness.